Pharm Res (2012) 29:1658–1669
DOI 10.1007/s11095-012-0690-z

RESEARCH PAPER

Hepatocellular Necrosis, Fibrosis and Microsomal Activity Determine the Hepatic Pharmacokinetics of Basic Drugs in Right-Heart-Failure-Induced Liver Damage

Peng Li • Thomas A. Robertson • Qian Zhang • Linda M. Fletcher • Darrell H. G. Crawford • Michael Weiss • Michael S. Roberts

Received: 6 November 2011 / Accepted: 17 January 2012 / Published online: 1 February 2012

ABSTRACT

Purpose To explore how liver damage arising from cardio-hepatic syndromes in RHF affect the hepatic pharmacokinetics of basic drugs.

Methods The hepatic pharmacokinetics of five selected basic drugs with different physicochemical properties were studied in IPRL from control rats and rats with RHF. Hepatic pharmacokinetic modelling was performed with a two-phase physiologically-based organ pharmacokinetic model with the vascular space and dispersion evaluated with the MID technique. The liver damage arising from RHF was assessed by changes in liver biochemistry and histopathology. The expression of various CYP isoforms was evaluated by real-time RT-PCR analysis.

Results Four of the five basic drugs had a significantly lower E in RHF rat livers compared to the control rat livers. Hepatic pharmacokinetic analysis showed that both the CL_{int} and PS were significantly decreased in the RHF rat livers. Stepwise regression analysis showed that the alterations in the pharmacokinetic parameters (E, CL_{int} and PS) can be correlated to the observed histopathological changes (NI, CYP concentration and FI) as well as to the lipophilicity of the basic drugs ($\log P_{app}$).

Conclusions Serious hepatocellular necrosis and fibrosis induced by RHF affects both hepatic microsomal activity and hepatocyte wall permeability, leading to significant impairment in the hepatic pharmacokinetics of basic drugs.

KEY WORDS fibrosis index · hepatic pharmacokinetics · hepatocellular necrosis · *in situ* perfused rat liver · right heart failure

ABBREVIATIONS

ALP	alkaline phosphatase
ALT	alanine transaminase
AST	aspartate transaminase
CL_{int}	intrinsic elimination clearance
CV^2	normalized variance
CYP	cytochrome P450
E	hepatic extraction ratio
FI	fibrosis index
HDL	high density lipoprotein
IPRL	*in situ* perfused rat liver
K_v	apparent distribution ratio
$\log P_{app}$	apparent partition coefficient
MID	multiple indicator dilution
MTT	Mean transit time
NASH	non-alcoholic steatohepatitis
NI	necrosis index
PS	permeability-surface area product
RHF	right heart failure
RT-PCR	reverse transcription polymerase chain reaction

P. Li (✉) · T. A. Robertson · Q. Zhang · M. S. Roberts
Therapeutics Research Centre, School of Pharmacy & Medical Sciences
Division of Health Sciences, University of South Australia
Basil Hetzel Institute for Medical Research
Adelaide, SA 5001, Australia
e-mail: Peng.li@unisa.edu.au

P. Li · T. A. Robertson · Q. Zhang · M. S. Roberts
Therapeutics Research Centre, School of Medicine
The University of Queensland, Princess Alexandra Hospital
Woolloongabba, QLD 4102, Australia

L. M. Fletcher · D. H. G. Crawford
Department of Gastroenterology & Hepatology, School of Medicine
University of Queensland, Princess Alexandra Hospital
Brisbane, Australia

M. Weiss
Department of Pharmacology
Martin Luther University Halle-Wittenberg
06097 Halle, Germany

INTRODUCTION

Chronic heart failure is a systemic clinical syndrome which has a variety of effects on other organ systems (1,2). Liver damage and cardio-hepatic syndromes have been widely identified in patients with right heart failure (RHF) (2,3). During RHF, increased central venous pressure leads to liver congestion and central venous dilation, which may subsequently impair liver perfusion and cause liver ischemia and hepatocellular necrosis (3). Profound hepatocellular ischemia and necrosis can develop into cardiogenic ischemic hepatitis with increased collagen deposition in the hepatic sinusoids (4). Whilst the histopathological characteristics of liver damage and cardio-hepatic syndromes during RHF are well described, it is still unclear how these syndromes may influence drug disposition in the liver.

The effects of liver disease and aging on hepatic drug disposition have been recognized since the 1980s (5). Our previous research with IPRL showed that liver fibrosis, cirrhosis and non-alcoholic steatohepatitis (NASH) can significantly affect hepatic pharmacokinetics (6,7). In these studies, the altered pathological hepatocellular morphology and biochemistry due to the disease states and physicochemical properties of drugs were showed to be key determinants of hepatic pharmacokinetics. Ion-trapping and microsomal binding can affect hepatic drug disposition in liver disease states (8,9). Moreover, our recent work showed that altered CYP isoform expression and fat deposition also play important roles in hepatic drug elimination and distribution during NASH (9).

Our knowledge about how RHF may affect hepatic drug pharmacokinetics is still limited. The published work in this area is focused on the changes in hepatic CYP levels, such as the reduced enzyme content derived from liver congestion and reduction of oxygen reported by Ng *et al.* (10). The hepatic expression of CYP2D and CYP3A was also found to be decreased expression in patients with RHF (11). Moreover, another study by Ng *et al.* (12) also reported the alteration in hepatic content, activity and latency of uridine diphosphate-glucuronosyltransferase in RHF. However, the variety of liver damage and cardio-hepatic syndromes during RHF, including hepatocellular necrosis, liver fibrosis and ischemia (13–15), could lead to significant alteration in hepatic drug disposition. It is still unclear how these syndromes may affect individual hepatic pharmacokinetics.

The aim of the current work is to explore how the liver damage due to RHF affects the hepatic pharmacokinetics of basic drugs and to relate the changes in individual pharmacokinetic processes, such as hepatocyte membrane permeability and intrinsic metabolic clearance, with the pathophysiological damage and physicochemical properties of these drugs. The hepatic pharmacokinetics of five selected basic drugs, including propranolol, labetalol, metoprolol, antipyrine and atenolol, which have different physicochemical properties (varying in pKa and lipophilicity), were studied with IPRL model in both healthy rats and rats with RHF. The RHF rat model was established through a single intraperitoneal injection dose of monocrotaline. In this model, the monocrotaline can selectively injure the vascular endothelium of the lung and induce pulmonary vasculitis, which then leads to pulmonary hypertension and finally progresses to RHF (16). The IPRL-coupled MID method enables the characterization of hepatic pharmacokinetic processes without recirculation effects and has been applied previously to studies of the hepatic pharmacokinetics of basic drugs in diseased livers (6,9). The perfusate outflow data were analyzed by a convection dispersion model that was coupled with a two-phase (sinusoids and hepatocytes) physiologically based organ pharmacokinetic model. The evolution of this combined model has been previously used to describe drug transfer across the hepatocyte membrane, intracellular distribution and elimination kinetics (17,18) and recently reviewed (19). Changes in hepatocellular histopathology (fibrosis index (FI) and necrosis index (NI)) and hepatic biochemistry (e.g., CYP isoform concentrations) were also characterised in both normal and RHF rat livers, and were used to define the mechanisms by which the liver damage due to RHF affected drugs' hepatic pharmacokinetics.

MATERIALS AND METHODS

Chemicals

Propranolol, labetalol, metoprolol, antipyrine and atenolol were all purchased from Sigma Aldrich (St. Louis, MO). Physicochemical properties of the selected drugs are summarized in Table I. [^{14}C] sucrose and [^{3}H] water were purchased from PerkinElmer Life and Analytical Sciences (Waltham, MA). All other chemicals used in this work were obtained from Sigma Aldrich (St. Louis, MO).

Rat Model of RHF

Briefly, male Wistar rats (approximately 250 g) were assigned to two groups: control group and RHF group. All rats were fed with standard rat chow and water. Body weight, food intake and water intake were monitored daily for rats in both groups for the duration of the experiment. The rat model of RHF was established using a single intraperitoneal dose of monocrotaline (60 mg/kg), as previously described (20). The control group was intraperitoneally injected with an equivalent volume of saline. Rats with RHF were monitored very closely for the first 24 hr, and then on a daily basis for 3–4 weeks duration. After 4 weeks,

Table I Physicochemical Properties of the Basic Drugs

Drugs	Molecular weight	$\log P_{app}$ [a]	f_{uB} [b]	pK_a [c]	Metabolising enzyme
Propranolol	259.34	3.10	0.69	9.45	CYP2D2
Labetalol	328.41	2.69	0.57	7.4	glucuronosyl transferase
Metoprolol	267.36	1.79	0.76	9.17	CYP2D2/3A2
Antipyrine	188.23	0.33	1.00	1.45	CYP3A2
Atenolol	266.34	0.14	0.47	9.6	CYP2D2

[a] Log octanol/water partition coefficient at pH 7.4 values (22)

[b] Fraction unbound in perfusate acquired with microfiltration method (9)

[c] Negative logarithm of the ionization constant

the rats were sacrificed to conduct the IPRL and histopathological studies. All animal studies were carried out following the protocols approved by the University of Queensland Animal Ethics Committee.

Liver Biochemistry Determination

Liver biochemistry function tests of the control rats and RHF models rats were performed at the Pathology Laboratory of the Princess Alexandra Hospital (Brisbane, Australia). Serum aspartate transaminase, alanine transaminase, alkaline phosphatise, total bilirubin and albumin were measured by a Synchron LX®20 Clinical System (Beckman Coulter, Fullerton, CA).

IPRL

The IPRL preparation used in this study was performed as described previously (21,22). A Wistar rat was anesthetized by intraperitoneal injection of xylazine at 10 mg/kg (Bayer Australia, Pymble, NSW, Australia) and ketamine-hydrochloride at 80 mg/kg (Parnell Laboratories, Alexandria, NSW, Australia), and followed with laparotomy. The animal was then heparinized (heparin sodium; David Bull Laboratories Australia, Mulgrave, Victoria, 200 units) via the inferior vena cava, and the bile duct was cannulated with PE-10 tubing (Becton Dickinson and Company, Sparks, MD). The portal vein was cannulated using a 16-gauge intravenous catheter and the liver was then perfused via this cannula with MOPS buffer, which contained 2% BSA and 15% prewashed canine red blood cells (RBCs) (Veterinary Specialist Services Pty Ltd, Brisbane, Australia) at pH 7.4 (21). The perfusion was conducted at 15 mL/min in each liver to reflect *in vivo* hepatic microcirculation. The perfusion medium was pumped with a peristaltic pump (Cole-Palmer, Vernon Hills, HL) and oxygenated using a silastic tubing lung ventilated with 100% pure oxygen (BOC Gases Australia, Brisbane, QLD). The rat was then sacrificed by thoracotomy and the thoracic inferior vena cava was cannulated within a PE-240 tubing (Becton Dickinson and Company, Sparks, MD). The animal was placed in a temperature-controlled cabinet with temperature set at 37° C. The total perfusion time for each liver was less than 2 h. Liver viability was evaluated by oxygen consumption, portal vein pressure, bile flow and macroscopic appearance as previously described by Cheung *et al.* (21).

Bolus Injection Study

The perfused liver was allowed to stabilize for 10 minutes before performing the MID study. For MID, aliquots (50 μL) of perfusion medium which contained [^{14}C] sucrose (1.5×10^5 dpm) and [^{3}H] water (3×10^5 dpm) were bolus injected into the liver. The outflow samples were collected by a fraction collector over 4 minutes. Aliquots of the basic drugs (8 mM propranolol, 6 mM labetalol, 3 mM metoprolol, 4 mM antipyrine, 4 mM atenolol approximately) were bolus injected into the liver separately and followed with sample collection over 4 min. In each liver, the order of injection was randomized and there was no repetition of the same injection in the same rat liver. A wash out and stabilization period of about 10 min was applied after every injection. All these outflow samples were centrifuged and aliquots (100 μL) of supernatant were taken for the sample analysis.

Analytical Procedure

The MID samples which contain [^{14}C] sucrose and [^{3}H] water were analyzed with a MINAXI beta TRICARB 4000 series liquid scintillation counter (Packard Instruments, Meriden, CT). The outflow samples for different basic drugs were determined with established HPLC methods which we have described and validated previously (22).

Histopathology Examination and Quantitation of Histology Index

Three to five slices of tissue were selected randomly from each liver and fixed in 10% neutral buffered formalin and then embedded in paraffin. Sections of 5 μm thickness were prepared and stained with hematoxylin-eosin (H&E) and Sirius Red to determine the degree of hepatocellular necrosis, liver fibrosis and inflammation. The light microscopy digital images were acquired with a ScanScope digital slide scanner (Aperio Technologies, Vista, CA) at the Pathology Laboratory of the Queensland Institute of Medical Research. The hepatocellular necrosis and liver fibrosis were quantified as NI and FI, respectively, with computer-assisted

image analysis (Image Scope version 10, Aperio Technologies, Vista, CA). For each rat, the area of necrotic hepatocytes and stained fibrotic tissue in five randomly selected fields was measured on the binary image. The FI was quantified from the total area of fibrosis divided by the total area of the section, as described previously (23). The necrosis index was the total area of necrotic hepatocytes divided by the total area of the selected section.

Determination of Liver CYP Concentration

Rat livers were harvested from the sacrificed rat and perfused with a mixed solution of calcium and magnesium-free Hank's balanced salt solution (5 mM EDTA and 10 mM HEPES) at 15 mL/min for 5 minutes to remove protein and blood from the sinusoid bed through the portal vein. The liver was then snap frozen in liquid nitrogen and stored at −80°C until analysis. The liver tissue (1 g) was then thawed and homogenized in 2.5 mL of ice-cold 0.25 M sucrose containing 50 mM Tris-HCl buffer (pH 7.4) using a tissue homogenizer. Then a gradient centrifugation was performed on the liver homogenates to separate the liver microsome fraction, as previously described (7). The CYP concentration in the microsome fraction was determined by the dithionite-reduced difference spectrum of CO-bubbled samples using the molar extinction difference at the peak position (~450 nm) (24).

Real-Time Reverse Transcription Polymerase Chain Reaction (RT-PCR) Analysis

The RNA was extracted from liver tissue using TRIzol reagent (Invitrogen, Mt. Waverley, Australia). The RNA concentration was measured by spectrophotometry. DNA within the RNA sample was removed by DNase treatment. First-strand cDNA was the synthesised from 1 g total RNA using SuperScript III Reverse Transcriptase (Invitrogen, Mt. Waverley, Australia) and oligo (dT(15)), according to the manufacturer's instructions.

Primers of CYP enzymes and a control housekeeping gene (*Gapdh*) were designed using Primer 3 software (Whitehead Institute for Biomedical Research, Cambridge, MA). The gene sequences for each forward and reverse primer are listed in Table II. The real-time RT-PCR amplifications were performed with a Corbett Rotor Gene 3000 (QIAGEN, Doncaster, VIC, Australia). The reactions were carried out in a total volume of 20 μL, with 400 nM forward primer, 400 nM reverse primer, 12.5 ng cDNA, and 10 μL QuantiTect SYBR Green PCR master mix (QIAGEN, Clifton Hill, Australia). The mRNA level was normalized with the housekeeping gene expression as an external standard and quantified by using the standard curve method. The result for each sample was expressed as a percentage when compared with gene expression in the liver from control rats.

Model Fitting of the Outflow Concentration-Time Profiles

Model fitting was performed by using the convection - dispersion model coupled with a two-phase physiologically based organ pharmacokinetic model, as previously described (22). The stochastic approach represents the transit of a molecule through the organ as a series of sojourns as shown in Fig. 1. The apparent distribution ratio between cellular and extracellular space (K_v) for the unbound solute is defined by k_{in}/k_{out}. The cellular binding processes were assumed to be one rapid and one slow dissociation process, respectively. The rapid binding process was simplified to an instantaneous equilibration process characterized by $K_R = k_{on,R}/k_{off,R}$. The slow binding process was described with the intracellular binding (k_{on}) and unbinding rate constant (k_{off}), respectively. The intrinsic elimination clearance (CL_{int}) and cellular water volume (V_c) determines the elimination rate constant $k_e = CL_{int}/V_c$. The permeation rate constant k_{in} is determined as: $k_{in} = (f_{uB} * PS)/V_B$, PS is the permeability-surface product and f_{uB} is the free fraction of solute in the perfusate. As previously described (25,26), the density of cellular residence times $\widehat{f_y}(s)$ describes the hepatocellular distribution and elimination kinetics (Eq. 1):

$$\widehat{f_y}(s) = \frac{k_{out}(s + k_{off})}{s^2(1 + K_R) + s\left(k_{off} + K_R k_{off} + k_e + k_{on} + k_{out}\right) + k_{off}(k_e + k_{out})} \quad (1)$$

The hepatic transit time density function $\widehat{f}(s)$ of solutes can be evaluated in terms of the extracellular transit time density of a nonpermeating reference molecule (in this study, sucrose) (Eq. 2).

Table II Primer Sequence for Real-Time RT-PCR Analysis of mRNA Expression

Primer name	Accession number	Forward primer	Reverse primer
Cyp3a2	NM_153312	CTGACAGACAAGCAGGGATG	TGGGTTCCAAGTCGGTAGAG
Cyp2d2	NM_012730	TGAGGACCCTTTCTTCAACAG	AGAATTGGGATTGCGTTCAG
Gapdh	NM_017008	GATGGTGAAGGTCGGTGTG	ATGAAGGGGTCGTTGATGG

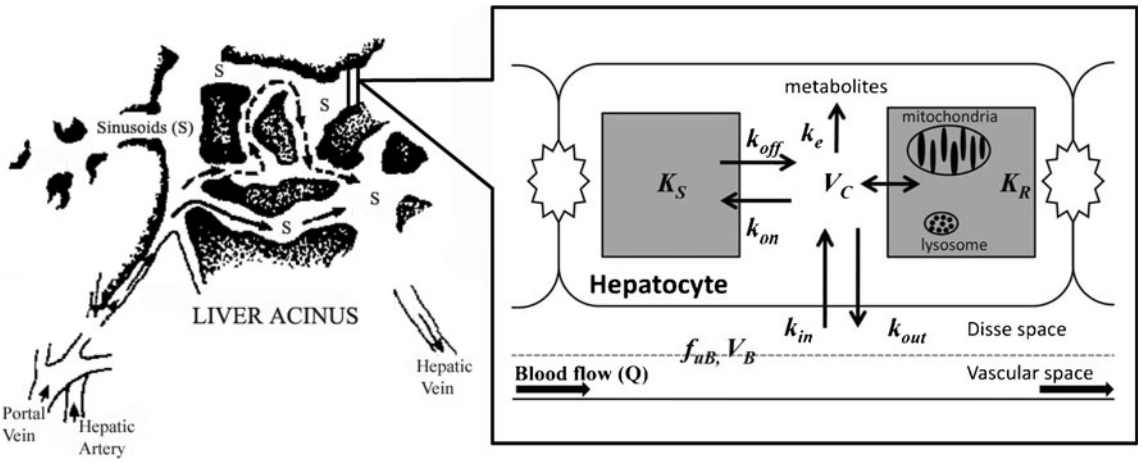

Fig. 1 Schematic overview of the two compartment convection dispersion model applied to transporter substrates disposition in the liver (9). k_{in}, influx rat constant; k_{out}, efflux rat constant; k_{in}/k_{out} defines the apparent distribution ratio between cellular and extracellular space (K_v) for the unbound solute; k_e elimination rat constant; K_R, equilibrium amount ratio charactering the fast binding process; k_{on}, k_{off}, rate constant for drug transport from cytosol into slow binding site which determines the equilibrium amount ratio K_S ($K_S = k_{on}/k_{off}$) that characterized the slow binding process.

$$\hat{f}(s) = \hat{f}_B[s + k_{in}\left(1 - \hat{f}_y(s)\right)] \tag{2}$$

The fractional outflow *versus* time data were fitted in the time domain by applying a numerical inverse Laplace transformation of the appropriate transit time density function using the nonlinear regression program SCIENTIST (MicroMath Scientific Software, Salt Lake City, UT).

Estimation of Nonparametric Pharmacokinetic Parameters

Nonparametric estimates of hepatic pharmacokinetic parameters including hepatic availability (F), mean transit time (MTT) and normalized variance were determined from the outflow concentration-time profiles for reference from Eqs. 3 and 4 by using the trapezoidal method (extrapolated to infinity) with exponential tail approximation.

$$F = \frac{Q \cdot AUC}{D} \tag{3}$$

$$MTT = \frac{\int_0^\infty tC(t)dt}{AUC} \tag{4}$$

$AUC = \int_0^\infty C(t)dt$ is the area under the solute concentration *versus* time curve, Q is the perfusate flow rate, D is the dose of solute administered and $\int_0^\infty tC(t)dt$ is the area under the first moment C(t) *versus* time curve. The areas beyond the last time point collected to time infinity was determined using expressions based on the terminal rate constant and concentration at the last time point for each curve. The hepatic extraction ratio (E) equals to 1-F.

Statistical Analysis

All data are presented as mean ± standard deviation unless otherwise stated. Statistical analysis was performed with two-way analysis of variance, student's *t*-test, ANOVA and linear regression analysis (where appropriate). Stepwise regression analysis was performed with SPSS 14.1 for Windows (SPSS Inc, Chicago, IL) and $p<0.05$ was taken as significant. Linear regression equations have only been considered when $r^2>0.5$. Correlation analysis between two parameters was performed with SPSS 14.1 for windows (SPSS Inc, Chicago, IL) to assess the Pearson's product-moment correlation coefficient and $p<0.05$ was taken as a significant correlation.

RESULTS

From the third to fourth week after monocrotaline injection, the RHF model rats started to show signs of illness due to the development of congestive heart failure. Liver physiology parameters from both control and RHF rats are listed in Table II. The RHF group showed significantly lower final body weight, as compared to the control group which is consistent with a previous work (20). The liver wet weight also showed a slight increase in the RHF group. Conversely, the rats of the RHF group showed significantly increased right ventricular and lung weight than the control rats. The central venous pressure was also significantly increased in the RHF rats. These syndromes suggest an impaired right ventricular function and blood recirculation consistent with the progression of RHF. There were no

significant differences detected in perfusion pressure, bile flow and oxygen consumption between the control and RHF groups in the IPRL experiment.

The serum biochemistry parameters of the control and RHF model rats are summarized in Table IV. The RHF group did not show significantly higher ALP, AST and ALT than the control group. However, the RHF model rats showed a significantly higher total bilirubin level ($P<0.05$). Representative liver sections of H&E stained liver slides acquired from control and RHF rats are shown in Fig. 2. Liver sections from the normal livers show typical architecture under light microscopy, while the liver sections from rats with RHF show serious central lobular necrosis and sinusoid dilation. Serious collagen deposition was also found within the sinusoid of RHF model rats. The estimated NI and FI are shown in Table IV. The liver sections from RHF rats show significantly higher FI and NI than those from control rats. Furthermore, the RHF rat livers also showed significantly decreased CYP concentration, as reflected in Table IV. Consistent with the decreased total CYP concentration, the mRNA expression of *Cyp3a2* is significantly lower in the RHF rat livers compared to the control rat livers, as shown in Fig. 3. Moreover, it also showed a highly suggestive reduction (without statistical significance) in the expression of *Cyp2d2* in the RHF rat livers compared to the control rat livers.

The representative outflow perfusate concentration - time profiles for each basic drug in the control and RHF rats are shown in Fig. 4, and Table V lists the nonparametric pharmacokinetic parameters for these basic drugs derived from the outflow profiles. The RHF group show significantly decreased E for these basic drugs other than for propranolol. The E of drugs increased with drug lipophilicity, as defined by the logarithm of their octanol-water partition coefficient ($\log P_{app}$). The MTT values for all five drugs did not differ significantly between the two groups. These outflow data were well fitted using a heterogeneous (barrier-limited and space-distributed) transit time model and a data weighting of $1/(y_{obs})^2$, as the nonlinear regression lines demonstrated in Fig. 4. The

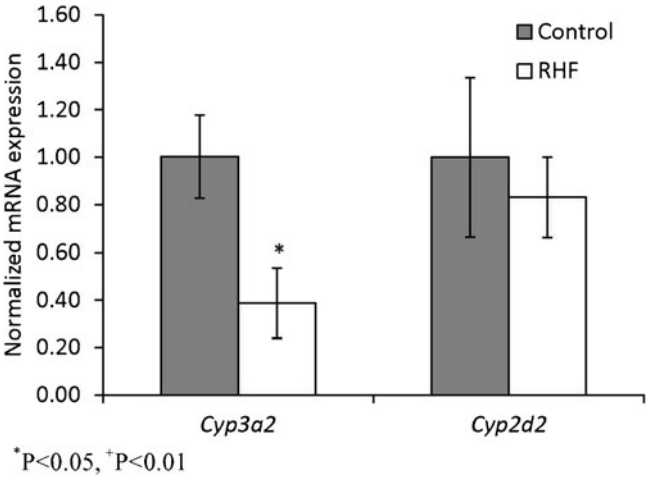

Fig. 3 mRNA expression of cyp3a2 and cyp2d2 in control and RHF rat livers.

pharmacokinetic parameters for each drug acquired from the model fitting are summarized in Table VI.

Both PS and CL_{int} for each drug were significantly decreased in the RHF group compared to the control group (Table VI). However, there was no significant change in K_v values for these drugs identified between the two groups. When comparing across different drugs, those with higher lipophilicity, as defined by $\log P_{app}$, show larger PS and CL_{int} values (Fig. 5), whereas those showing higher ionisation at physiological pHs (i.e. at higher pKa values, noting that antipurine with a pKa of 1.5 is essentially unionised at both the organelle pH of ~4 and physiological pH of ~7.4) are associated with more ion trapping and increasing in K_v values (Fig. 5). Stepwise regression analysis, which was used to examine the relationships among pharmacokinetic parameters ($\log PS$ and $\log CL_{int}$), drug physicochemical properties ($\log P_{app}$) and histopathological results (FI, NI and CYP), yielded the following relatioships:

1) $\log PS = 0.769 - 0.097 * \log FI + 0.203 * \log P_{app} (r^2 = 0.812,\ n = 30,\ p < 0.001)$

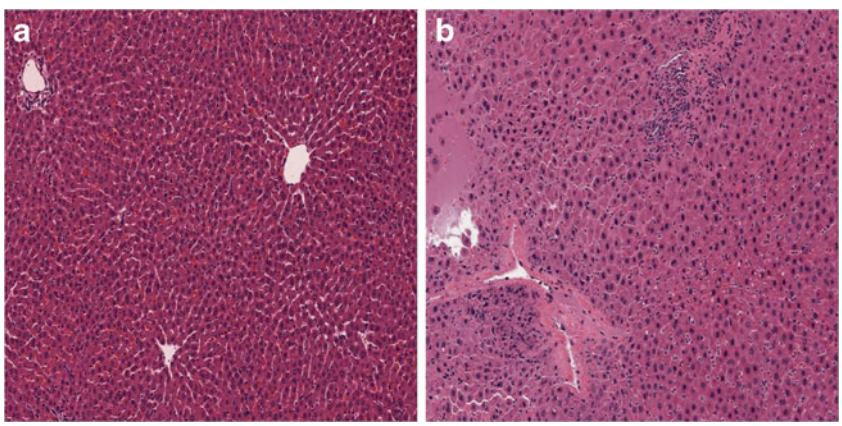

Fig. 2 Representative liver sections from the control and RHF rats (H&E stain) (**a**) control (X200). (**b**) RHF (X200).

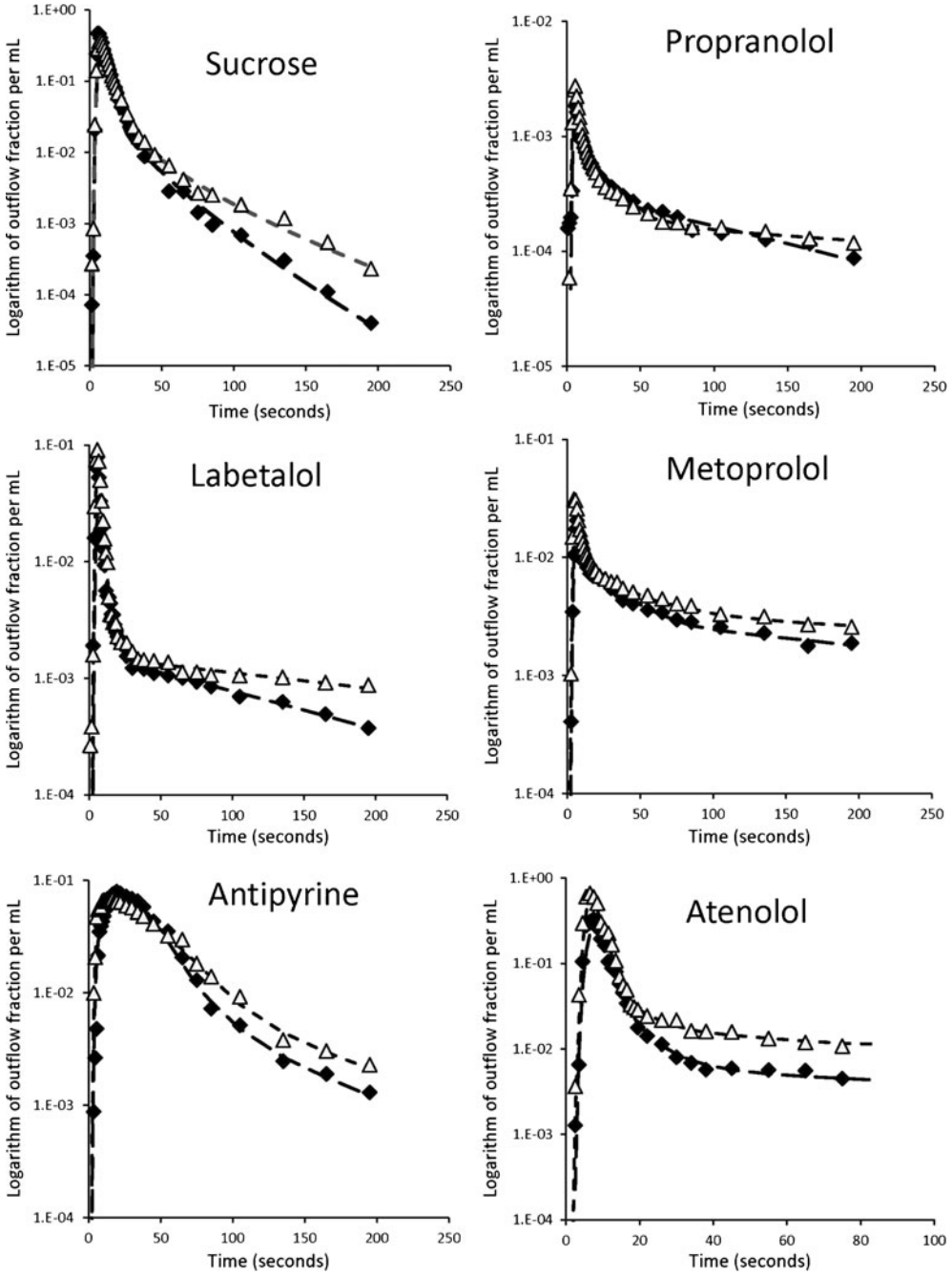

Fig. 4 Representative outflow perfusate concentration – time profiles for the basic drugs in control (*filled diamond*) and RHF (*empty triangle*) rats.

2) $\log CL_{int} = -4.097 + 1.639 * \log\mathrm{CYP} + 0.478 * \log P_{\mathrm{app}} (r^2 = 0.779,\ n = 30,\ p < 0.001)$

3) $\log E = -0.476 - 0.202 * \log\mathrm{CYP} - 0.211 * \log\mathrm{NI} + 0.355 * \log P_{\mathrm{app}} (r^2 = 0.854, n = 30, p < 0.001)$

Comparisons between the observed and predicted pharmacokinetic parameters for the various bases are shown in Fig. 6. The predicted pharmacokinetics parameters, including log*PS*, logCL_{int}, and *E*, all correlated well with the estimated parameters from the IPRL study.

DISCUSSION

In this work, the monocrotaline-induced rat model of RHF was established to study potentially altered RHF induced hepatic drug disposition due to liver damage. The rats in the RHF group started to show signs of illness and significantly decreased body weight from the third to fourth week after monocrotaline injection, consistent with a previous report (20). A significantly increased central venous pressure, as well as an increased

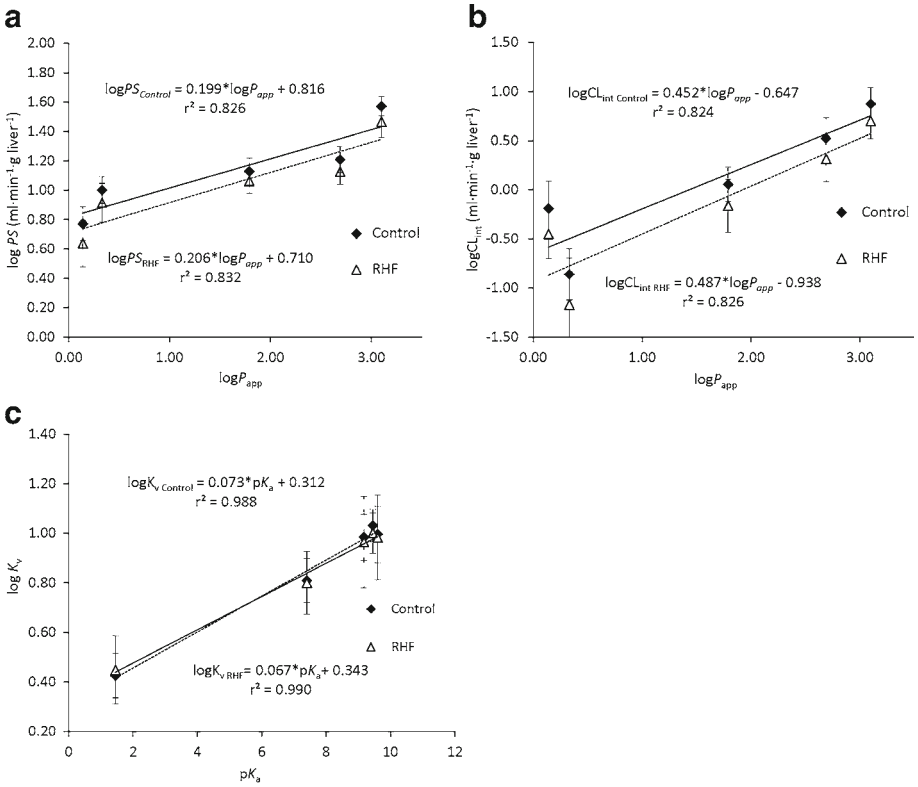

Fig. 5 Relationship between physicochemical properties and their hepatic pharmacokinetic parameters for basic drugs in control and RHF rats. (**a**) Logarithm of octanol/water partition coefficient (logP_{app}) for basic drugs and the log*PS*, (**b**) logarithm of octanol/water partition coefficient (logPapp) of these drugs and log CL_{int}, (**c**) pKa of these drugs and logK_v. The line represents the linear regression line. The data are represented as the mean ± S.D.

right ventricular and lung weight (Table III), indicated serious heart and lung damage and suggested the successful establishment of the RHF model (16). A potential confounder in the use of monocrotaline induced RHF is a direct effect of monocrotaline on the liver itself (27,28). However, dose range studies show that such

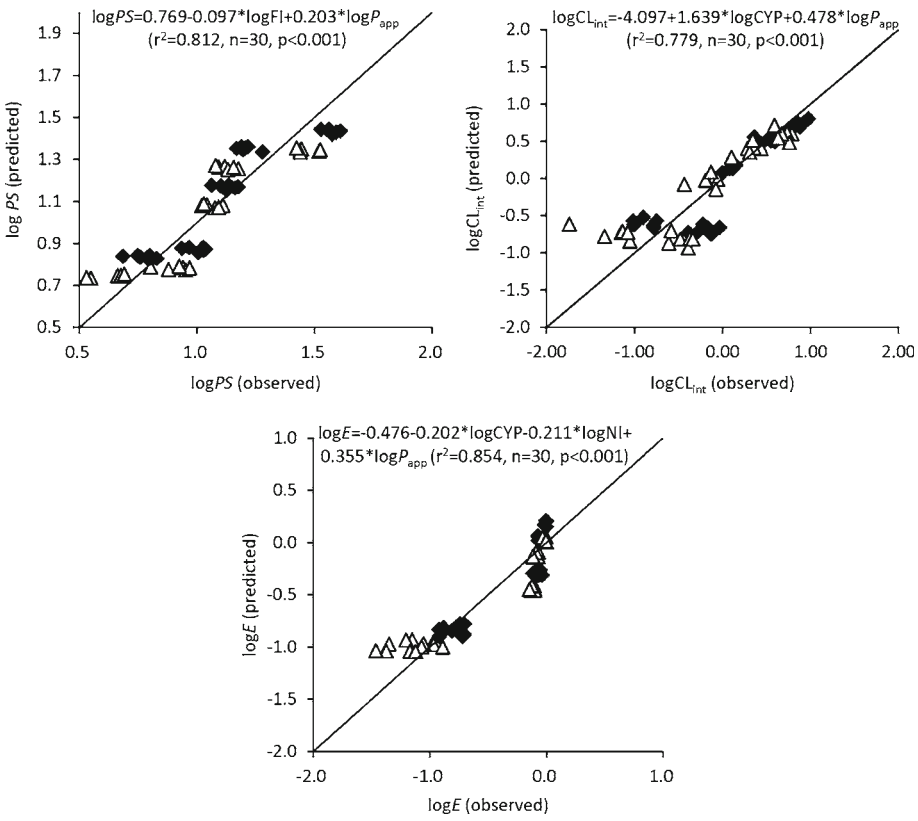

Fig. 6 Comparison of observed and predicted pharmacokinetic parameters for basic drugs in control (*filled diamond*) and right heart failure (RHF) (*empty triangle*) rat liver.

Table III Comparison of Liver Perfusion Parameters Between Control and RHF Rats (mean ± S.D., $n=6$)

Perfusion parameters	Animal model	
	Control rats	RHF rats
Final rat body weight (g)	355 ± 22	315 ± 17*
Liver wet weight (g)	10.36 ± 1.31	11.31 ± 0.96
Lung weight (g)	1.57 ± 0.12	3.06 ± 0.76+
Right ventricular weight (g)	0.33 ± 0.04	0.51 ± 0.08+
Central venous pressue (mm Hg)	22 ± 8	50 ± 12+
Perfusion rate (ml·min^{-1}·g liver^{-1})	1.47 ± 0.19	1.33 ± 0.10
Perfusion pressure (cmH_2O)	26.00 ± 2.21	29.50 ± 1.38
Bile flow, μl·min^{-1}·g liver^{-1}	0.83 ± 0.13	0.80 ± 0.15
O_2 consumption, μmol·min^{-1}·g liver^{-1}	2.18 ± 0.44	1.92 ± 0.51

* $P<0.05$, + $P<0.01$

damage occurs at 200–300 mg/kg about 4 times the dose (60 mg/kg) used in this study (27,28).

Histological examination confirmed the serious hepatocellular necrosis and liver fibrosis injury which were demonstrated as significantly increased NI and FI in the rat livers of the RHF group (Table IV). The central venous congestion injury also leads to a significantly higher serum bilirubin level and slightly increased serum albumin concentration in the RHF model rats (4). However, there was no significant change in the liver perfusion parameters including perfusion pressure, bile flow and oxygen consumption, detected between the two experimental groups. The RHF group also did not show a significant increase in ALP, AST and ALT levels compared with the control group. These results are consistent with other published studies (2,29), and indicate that the liver damage at this stage of RHF was not serious enough to significantly influence the serum biochemistry level.

Moreover, the significantly decreased total liver CYP concentration in the RHF model rats (Table IV) is consistent with previous results (14,15,30) which also observed decreased CYP expression. The decreased CYP concentration suggested the serious damage with liver oxidative metabolism during the progression of right heart failure and the consequent hepatic congestion and ischemia. The reduced total CYP concentration in the RHF group was also consistent with the decreased mRNA expression of *Cyp2d2* and *Cyp3a2* identified by the real time RT-PCR experiment. Reduction in CYP2D and CYP3A expression in human patients during acute hypoxia has also been reported (11).

As a consequence of liver damage during RHF, the E for four of the five basic drugs studied were significantly decreased in RHF rat livers compared to in control rat livers (Table V), with the exception of propranolol. This significantly reduced E is consistent with the results reported in previous studies. For instance, Petersson *et al.* (31) reported impaired nitroglycerin elimination in patients with chronic heart failure, whilst Ng *et al.* (12) showed a reduced hepatic elimination of p-nitrophenol in a rat model of RHF. Whilst these published studies recognized the reduced E values in the liver during RHF, the mechanism by which RHF induced liver damage led to the reduced E values was not well explored. The present work suggests that the significantly reduced E values arise from a significantly decreased intrahepatic clearance and hepatocyte membrane permeability, reflected by the significantly decreased values for PS and CL_{int} (Table VI) (6,32,33). From our previous studies, changes in E can be related to a number of determinants: the lipophilicity of the drugs, represented by logP_{app}, changes in FI and an altered CYP expression in the diseased liver (6,9). In this work, stepwise regression analysis identified the that RHF induced changes in extraction, expressed as log E to relate to the logarithm of other parameters, was mainly determined by logP_{app}, logNI and logCYP during RHF ($p<0.001$) and not by pK_a (Figs. 5 and 6). The predicted E values acquired from this regression showed a good correlation with the observed E values (Fig. 6). These results suggested that, except for the CYP concentration, the hepatocellular necrosis (NI), other than liver fibrosis (FI), is the key determinant of E during RHF. This result suggests that

Table IV Comparison of Serum Biochemical and Quantitative Liver Histopathological Parameters Between Control and RHF Rats (mean ± S.D., $n=6$)

Parameters	Control rats	RHF rats
ALP (IU/L)	81.15 ± 11.44	73.07 ± 9.25
AST (IU/L)	119.02 ± 7.76	123.38 ± 9.90
ALT (IU/L)	28.75 ± 3.00	31.48 ± 4.67
Bilirubin (umol/L)	7.55 ± 1.05	9.97 ± 1.02*
Albumin (g/L)	14.80 ± 1.53	13.03 ± 1.40
Fibrosis index (%)	0.42 ± 0.11	3.56 ± 0.61+
Necrosis index (%)	1.52 ± 0.39	9.40 ± 1.55+
CYP (nmol/g liver)	110.06 ± 7.81	91.04 ± 9.84 *

* $P<0.05$, + $P<0.01$

Table V Nonparametric Estimates of Basic Drug Pharmacokinetic Parameters (mean ± S.D., $n=6$)

Basic drugs	E (%)		MTT (s)	
	Control	RHF	Control	RHF
Propranolol	0.98 ± 0.02	0.96 ± 0.03	58.14 ± 5.10	59.30 ± 6.27
Labetalol	0.86 ± 0.02	0.80 ± 0.04*	29.10 ± 5.87	27.35 ± 2.07
Metoprolol	0.84 ± 0.05	0.76 ± 0.03*	60.26 ± 5.41	59.57 ± 3.61
Antipyrine	0.16 ± 0.03	0.08 ± 0.02+	46.46 ± 3.55	48.65 ± 6.74
Atenolol	0.16 ± 0.03	0.07 ± 0.03+	13.12 ± 2.27	12.67 ± 1.85

* $P<0.05$, + $P<0.01$

Table VI Kinetic Parameters Derived from Two-Phase Stochastic Model Fitting Basic Drugs in Livers from Normal and RHF Rats (mean ± S.D., $n=6$)

Drugs	$\log P_{app}$ [a]	pK_a [b]	*PS* (mL·min^{-1}·g liver)		K_v		CL_{int} (mL·min^{-1}·g liver)	
			Control	RHF	Control	RHF	Control	RHF
Propranolol	3.10	9.45	37.28 ± 2.43	29.27 ± 3.08^{+}	10.76 ± 1.40	10.02 ± 1.27	7.50 ± 1.26	5.02 ± 0.89^{+}
Labetalol	2.69	7.4	16.22 ± 1.46	13.38 ± 1.14*	6.45 ± 1.13	6.31 ± 0.44	3.34 ± 0.69	2.07 ± 0.49*
Metoprolol	1.79	9.17	13.43 ± 1.24	11.55 ± 0.97*	9.64 ± 1.07	9.22 ± 1.08	1.13 ± 0.20	0.69 ± 0.18^{+}
Antipyrine	0.33	1.45	10.01 ± 0.90	8.21 ± 1.08*	2.67 ± 0.22	2.81 ± 0.52	0.14 ± 0.04	0.06 ± 0.03^{+}
Atenolol	0.14	9.6	5.91 ± 0.67	4.34 ± 0.69^{+}	9.90 ± 0.92	9.61 ± 1.19	0.65 ± 0.18	0.35 ± 0.09^{+}

[a] log octanol/water partition coefficient at pH 7.4 values (22)

[b] negative logarithm of the ionization constant

$^{*}P<0.05$, $^{+}P<0.01$

the CYP concentration and hepatocellular necrosis may be used as predictors to evaluate the possible decrease of *E* during RHF. Therefore, a reduction in dosing may be required for patients with RHF who have been given hepatically cleared drugs.

In this work, we sought to dissect out the mechanisms by RHF induced liver damage caused a change in basic drug pharmacokinetics using linear and stepwise regression (Fig. 5). Both regression analyses confirmed our earlier work (6,9,22) that lipophilicity of these basic drugs ($\log P_{app}$) is a key determinant of CL_{int} and *PS*, whereas the pK_a value defines the ion-trapping in hepatocytes as determined by K_v. It is to be recognised that the lowest K_v for antipyrine (pK_a 1.5) represents the control case of no ion trapping as it is effectively unionised at the pH for the acidic organelles in hepatocytes as its pK_a is >2 pH units less than the organelle pH (22). The similar profiles of K_v *versus* pK_a with and without RHF, suggests that RHF has not induced any change in organelle pH.

The stepwise regression analysis in Fig. 6 also showed that the reduction in *PS* could be linearly related to the significantly increased FI arising from RHF effects on rat livers. The significance of this finding is the possibility of using FI as a predictor of liver function, especially changes in *PS*, after RHF induced liver damage. We have previously shown that FI is the main determinant of *PS* in fibrotic, cirrhotic, and NASH livers (6,9).

The lack of change in *E* for propranolol is consistent with this drug's hepatic clearance mainly be determined by hepatic blood flow because it is so highly extracted (34). This finding is consistent with a lack of change in *E* for propranolol in NASH liver rats (9). In each of these studies, an identical blood flow was used in the control and RHF IPRL studies. In reality, RHF is associated with a reduction in portal vein blood flows (35). Accordingly, as clearance can be defined as the product of hepatic blood flow and *E*, it is anticipated that propranolol's hepatic clearance will therefore be lower in RHF. Indeed, an impaired propranolol hepatic clearance has been reported in rat livers following RHF (10).

The significantly decreased CL_{int} values in the RHF rat livers for these basic drugs were also found to be related to the decreased total CYP concentration (Fig. 6), which are also consistent with an observed reduction in mRNA expression for *Cyp2d2* and *Cyp3a2*. These results indicate that the logarithm of CYP concentration may be one predictor for $\log CL_{int}$ (Fig. 6). As labetalol is also metabolized through glucuronidation, it is possible that the significant reduction in CL_{int} for labetalol may be due to reduced glucuronidation. However, previous studies suggested that there was no significant change in glucuronosyl transferase for rat livers with RHF (12).

It is recognised that the physiological pharmacokinetic model for the liver used here is limited by being dependent on interpreting intrahepatic events based on observed outflow profiles as we have reported in other studies (9,36,37) In principle, the model we have used can be improved by more precisely representing the liver *in silico* formally as consisting of a population of several thousand hepatocytes arranged into hepatic "lobules" according to vascular and biliary inputs and outputs and liver morphology, but this requires more intense computation (38,39). A much more precise method of analysing pharmacokinetic events in the liver and in other organs, e.g. the hindlimb (40) and skin (41) is to observe events directly in the vascular system and in cells. We are now attempting to develop non-invasive imaging of processes in the liver (42) to enable more precise characterisation of physiological pharmacokinetic events, including how drugs are transported in the liver's vascular system (43) and where in the liver drugs are taken up and converted to their metabolites (44,45).

CONCLUSION

This work shows that hepatic pharmacokinetics are significantly changed in rats with RHF. The altered hepatic pharmacokinetic parameters (*E*, CL_{int} and *PS*) can be related to the physicochemical properties of basic drugs ($\log P_{app}$) and

liver histopathological changes (NI, CYP concentration and FI) in the rat with RHF. These results add to our understanding of when and how liver damage due to the RHF affects drug hepatic pharmacokinetics. The results might also provide a possible way to predict the pharmacokinetic parameters from physicochemical properties and liver histopathology changes during RHF or liver ischemia injury. Conversely, these results also suggest that the level of liver histopathological damage may be evaluated from the hepatic pharmacokinetic study of specific probes.

ACKNOWLEDGMENTS & DISCLOSURES

This work was supported by the National Health and Medical Research Council of Australia (Grant 569710). We thank Dr. Clay Winterford for performing liver histopathology examination and Dr. Goce Dimeski for performing the serum biochemistry determinations.

REFERENCES

1. Felker GM, Allen LA, Pocock SJ, Shaw LK, McMurray JJ, Pfeffer MA, *et al.* Red cell distribution width as a novel prognostic marker in heart failure: data from the CHARM Program and the Duke Databank. J Am Coll Cardiol. 2007;50(1):40–7.
2. Allen LA, Felker GM, Pocock S, McMurray JJ, Pfeffer MA, Swedberg K, *et al.* Liver function abnormalities and outcome in patients with chronic heart failure: data from the Candesartan in Heart Failure: Assessment of Reduction in Mortality and Morbidity (CHARM) program. Eur J Heart Fail. 2009;11(2):170–7.
3. Giallourakis CC, Rosenberg PM, Friedman LS. The liver in heart failure. Clin Liver Dis. 2002;6(4):947–67. viii–ix.
4. Seeto RK, Fenn B, Rockey DC. Ischemic hepatitis: clinical presentation and pathogenesis. Am J Med. 2000;109(2):109–13.
5. Williams RL, Mamelok RD. Hepatic disease and drug pharmacokinetics. Clin Pharmacokinet. 1980;5(6):528–47.
6. Hung DY, Chang P, Cheung K, McWhinney B, Masci PP, Weiss M, *et al.* Cationic drug pharmacokinetics in diseased livers determined by fibrosis index, hepatic protein content, microsomal activity, and nature of drug. J Pharmacol Exp Ther. 2002;301 (3):1079–87.
7. Hung DY, Chang P, Cheung K, Winterford C, Roberts MS. Quantitative evaluation of altered hepatic spaces and membrane transport in fibrotic rat liver. Hepatology. 2002;36(5):1180–9.
8. Siebert GA, Hung DY, Chang P, Roberts MS. Ion-trapping, microsomal binding, and unbound drug distribution in the hepatic retention of basic drugs. J Pharmacol Exp Ther. 2004;308(1):228–35.
9. Li P, Robertson TA, Thorling CA, Zhang Q, Fletcher LM, Crawford DH, *et al.* Hepatic pharmacokinetics of cationic drugs in a high-fat emulsion-induced rat model of nonalcoholic steatohepatitis. Drug Metabol Dispos. 2011;39(4):571–9.
10. Ng CY, Ghabrial H, Morgan DJ, Ching MS, Smallwood RA, Angus PW. Impaired elimination of propranolol due to right heart failure: drug clearance in the isolated liver and its relationship to intrinsic metabolic capacity. Drug Metab Dispos. 2000;28 (10):1217–21.
11. Jurgens G, Christensen HR, Brosen K, Sonne J, Loft S, Olsen NV. Acute hypoxia and cytochrome P450-mediated hepatic drug metabolism in humans. Clin Pharmacol Ther. 2002;71(4):214–20.
12. Ng CY, Ghabrial H, Morgan DJ, Ching MS, Smallwood RA, Angus PW. Right heart failure impairs hepatic elimination of p-nitrophenol without inducing changes in content or latency of hepatic UDP-glucuronosyltransferases. J Pharmacol Exp Ther. 2000;295(2):830–5.
13. Baughman Jr RA, Arnold S, Benet LZ, Lin ET, Chatterjee K, Williams RL. Altered prazosin pharmacokinetics in congestive heart failure. Eur J Clin Pharmacol. 1980;17(6):425–8.
14. Angus PW, Ng CY, Ghabrial H, Morgan DJ, Smallwood RA. Effects of chronic left ventricular failure on hepatic oxygenation and theophylline elimination in the rat. Drug Metab Dispos. 1995;23(4):485–9.
15. Jones DP. Hypoxia and drug metabolism. Biochem Pharmacol. 1981;30(10):1019–23.
16. Hessel MH, Steendijk P, den Adel B, Schutte CI, van der Laarse A. Characterization of right ventricular function after monocrotaline-induced pulmonary hypertension in the intact rat. Am J Physiol. 2006;291(5):H2424–30.
17. Weiss M, Stedtler C, Roberts MS. On the validity of the dispersion model of hepatic drug elimination when intravascular transit time densities are long-tailed. Bull Math Biol. 1997;59(5):911–29.
18. Weiss M, Roberts MS. Tissue distribution kinetics as determinant of transit time dispersion of drugs in organs: application of a stochastic model to the rat hindlimb. J Pharmacokinet Biopharm. 1996;24(2):173–96.
19. Roberts MS. Drug structure-transport relationships. J Pharmacokinet Pharmacodyn. 2010;37(6):541–73.
20. Pasini E, Cargnioni A, Pastore F, Razzetti R, Bongrani S, Gitti GL, *et al.* Effect of nolomirole on monocrotaline-induced heart failure. Pharmacol Res. 2004;49(1):1–5.
21. Cheung K, Hickman PE, Potter JM, Walker NI, Jericho M, Haslam R, *et al.* An optimized model for rat liver perfusion studies. J Surg Res. 1996;66(1):81–9.
22. Hung DY, Chang P, Weiss M, Roberts MS. Structure-hepatic disposition relationships for cationic drugs in isolated perfused rat livers: transmembrane exchange and cytoplasmic binding process. J Pharmacol Exp Ther. 2001;297(2):780–9.
23. O'Brien MJ, Keating NM, Elderiny S, Cerda S, Keaveny AP, Afdhal NH, *et al.* An assessment of digital image analysis to measure fibrosis in liver biopsy specimens of patients with chronic hepatitis C. Am J Clin Pathol. 2000;114(5):712–8.
24. Matsubara T, Koike M, Touchi A, Tochino Y, Sugeno K. Quantitative determination of cytochrome P-450 in rat liver homogenate. Anal Biochem. 1976;75(2):596–603.
25. Weiss M, Kuhlmann O, Hung DY, Roberts MS. Cytoplasmic binding and disposition kinetics of diclofenac in the isolated perfused rat liver. Br J Pharmacol. 2000;130(6):1331–8.
26. Weiss M. Cellular pharmacokinetics: effects of cytoplasmic diffusion and binding on organ transit time distribution. J Pharmacokinet Biopharm. 1999;27(3):233–56.
27. Joseph B, Kumaran V, Berishvili E, Bhargava KK, Palestro CJ, Gupta S. Monocrotaline promotes transplanted cell engraftment and advances liver repopulation in rats via liver conditioning. Hepatology. 2006;44(6):1411–20.
28. Copple BL, Roth RA, Ganey PE. Anticoagulation and inhibition of nitric oxide synthase influence hepatic hypoxia after monocrotaline exposure. Toxicology. 2006;225(2–3):128–37.
29. Nishi H, Takahashi T, Ichikawa H, Matsumiya G, Matsuda H, Sawa Y. Prediction of postoperative hepatic dysfunction after cardiac surgery in patients with chronic congestive heart failure. Gen Thorac Cardiovasc Surg. 2009;57(7):357–62.
30. Ng CY, Angus PW, Ghabrial H, Chou ST, Arnolda L, Morgan DJ, *et al.* Right heart failure impairs hepatic oxygenation and

theophylline clearance in rats. J Pharmacol Exp Ther. 1995;273 (3):1332–6.
31. Petersson M, Rundqvist B, Bennett BM, Adams MA, Friberg P. Impaired nitroglycerin biotransformation in patients with chronic heart failure. Clin Physiol Funct Imaging. 2008;28(4):229–34.
32. Roberts MS, Anissimov YG. Modeling of hepatic elimination and organ distribution kinetics with the extended convection-dispersion model. J Pharmacokinet Biopharm. 1999;27(4):343–82.
33. Roberts MS, Rowland M. A dispersion model of hepatic elimination: 1. Formulation of the model and bolus considerations. J Pharmacokinet Biopharm. 1986;14(3):227–60.
34. Pang KS, Rowland M. Hepatic clearance of drugs. I. Theoretical considerations of a "well-stirred" model and a "parallel tube" model. Influence of hepatic blood flow, plasma and blood cell binding, and the hepatocellular enzymatic activity on hepatic drug clearance. J Pharmacokinet Biopharm. 1977;5(6):625–53.
35. Catalano D, Caruso G, DiFazzio S, Carpinteri G, Scalisi N, Trovato GM. Portal vein pulsatility ratio and heart failure. J Clin Ultrasound. 1998;26(1):27–31.
36. Roberts MS, Liu X, Zou Y, Siebert GA, Chang P, Whitehouse MW, *et al.* Effect of adjuvant-induced systemic inflammation in rats on hepatic disposition kinetics of taurocholate. Am J Physiol Gastrointest Liver Physiol. 2011;300(1):G130–6.
37. Weiss M, Li P, Roberts MS. An improved nonlinear model describing the hepatic pharmacokinetics of digoxin: evidence for two functionally different uptake systems and saturable binding. Pharm Res. 2010;27(9):1999–2007.
38. Yan L, Hunt CA, Ropella GE, Roberts MS. In silico representation of the liver-connecting function to anatomy, physiology and heterogeneous microenvironments. Conf Proc IEEE Eng Med Biol Soc. 2004;2:853–6.
39. Park S, Ropella GE, Kim SH, Roberts MS, Hunt CA. Computational strategies unravel and trace how liver disease changes hepatic drug disposition. J Pharmacol Exp Ther. 2009;328(1):294–305.
40. Wu ZY, Rivory LP, Roberts MS. Physiological pharmacokinetics of solutes in the isolated perfused rat hindlimb: characterization of the physiology with changing perfusate flow, protein content, and temperature using statistical moment analysis. J Pharmacokinet Biopharm. 1993;21(6):653–88.
41. Singh P, Roberts MS. Dermal and underlying tissue pharmacokinetics of salicylic acid after topical application. J Pharmacokinet Biopharm. 1993;21(4):337–73.
42. Roberts MS, Roberts MJ, Robertson TA, Sanchez W, Thorling C, Zou Y, *et al. In vitro* and *in vivo* imaging of xenobiotic transport in human skin and in the rat liver. J Biophotonics. 2008;1(6):478–93.
43. Bass L, Roberts MS, Robinson PJ. On the relation between extended forms of the sinusoidal perfusion and of the convection-dispersion models of hepatic elimination. J Theor Biol. 1987;126 (4):457–82.
44. Roberts MS, Donaldson JD, Rowland M. Models of hepatic elimination: comparison of stochastic models to describe residence time distributions and to predict the influence of drug distribution, enzyme heterogeneity, and systemic recycling on hepatic elimination. J Pharmacokinet Biopharm. 1988;16(1):41–83.
45. Roberts MS, Rowland M. A dispersion model of hepatic elimination: 3. Application to metabolite formation and elimination kinetics. J Pharmacokinet Biopharm. 1986;14(3):289–308.